

Interpretable Spatio-Temporal Features Extraction based Industrial Process Modeling and Monitoring by Soft Sensor

Qianchao Wang¹, Peng Sha², Leena Heistrene³, Yuxuan Ding^{1†}, Yaping Du¹,

Abstract—Data-driven soft sensors have been widely applied in complex industrial processes. However, the interpretable spatio-temporal features extraction by soft sensors remains a challenge. In this light, this work introduces a novel method termed spatio-temporal consistent and interpretable model (STCIM). First, temporal and spatial features are captured and aligned by a far topological spatio-temporal consistency extraction block. Then, the features are mapped into an interpretable latent space for further prediction by explicitly giving physical meanings to latent variables. The efficacy of the proposed STCIM is demonstrated through the modeling of two generated datasets and a real-life dataset of coal-fired power plants. The corresponding experiments show: 1) The generalization of STCIM outperforms other methods, especially in different operation situations. 2) The far topological spatio-temporal consistency is vital for feature alignment. 3) The hyper-parameters of physics-informed interpretable latent space loss decide the performance of STCIM.

Keywords—Power plant, Soft sensor, Deep-learning, physics-informed modeling

I. INTRODUCTION

PROCESS modeling and monitoring are the cornerstones of stable operation and security in large systems engineering. However, data offset, noise disturbance, low reliability of analyzers, and delays in long time-series data from most processes lead to a mismatch between models and the data, resulting in potential safety hazards and poor product quality. As a solution, soft sensors are used for process monitoring, quality prediction, and many other important applications [1].

There are two main types of approaches to establish soft sensing models, namely, mechanism-based [2] and data-driven methods [3], [4]. Mechanism-based methods, also called first-principle models, use physicochemical governing equations and dynamic differential equations to describe industrial processes. When the mechanism of the process is well understood or sufficient knowledge about the process is available, mechanism-based methods can work effectively. However, the complexity of large-scale industrial systems often makes these

preconditions difficult to meet, limiting the applicability of the first principles. In contrast, data-driven methods, particularly deep learning (DL), have achieved significant success in chemical, biochemical, and metallurgical processes, as they do not require extensive prior knowledge [5].

Due to the strong local spatio-temporal features of long time-series data in industrial processes, convolutional neural networks (CNNs) are widely applied in soft sensors for local feature learning [6]. For example, a variable correlation analysis-based CNN is proposed for topological feature extraction [7], [8], as demonstrated in the hydrocracking process and the debutanizer column. A dynamic CNN strategy is designed to learn hierarchical local nonlinear dynamic features for soft sensor modeling [9]. Furthermore, a multiscale attention-based CNN is proposed in [10] to extract multi-scale local features from complex multi-coupled process data. However, the inability of CNNs to capture global features and the potential far topological structure of variables limits the prediction accuracy of models. Hence, other deep learning models, such as long short-term memory (LSTM) [11], and transformers [12], [13] are applied in soft sensor. In [14], a novel multi-view spatial-temporal transformer network is proposed to learn complex spatial-temporal domain correlations and potential patterns from multiple views for accurate traffic-flow prediction. By incorporating an additional reconstruction constraint for the raw input data in each layer, a stacked enhanced auto-encoder is designed in [15] to learn features. However, the learned spatio-temporal features always assume spatio-temporal alignment, which ignores the time delays and coupling among variables, resulting in poor generalization.

Another problem is that these black-box models lack physical interpretability. The captured spatio-temporal features of long time-series data are sparse, which cannot be explained by first principles, limiting their practicality. Although graph neural networks are considered a way to incorporate prior knowledge into networks, they are used primarily to identify physical correlations among variables [16]–[18]. Fortunately, a potential solution to this problem lies in physics-informed or guided neural networks, which are designed to enhance the transparency and explainability of deep learning models (PINNs) [19], ensuring that their outputs adhere to physical laws [20]. By integrating differential equations and initial conditions into the loss function, these models leverage the automatic differentiation capability of neural networks while embedding fundamental physical laws [21]. They have been successfully applied to lake temperature prediction [22], pa-

Yuxuan Ding is the corresponding author

¹ Qianchao Wang, Yuxuan Ding, and Yaping Du is with the Department of Building Environment and Energy Engineering, Hong Kong Polytechnic University, Hung Hom, Hong Kong. (qianchao.wang@polyu.edu.hk; yx.ding@connect.polyu.hk; Ya-ping.du@polyu.edu.hk)

² Peng Sha is with Key Laboratory of Energy Thermal Conversion and Control of Ministry of Education, School of Energy and Environment, Southeast University, Nanjing, China. (sha_peng@seu.edu.cn)

³ Leena Heistrene is with Department of Electrical Engineering, School of Energy Technology, Pandit Deendayal Energy University, Gandhinagar, Gujarat, India. (leena.santosh@sof.pdpu.ac.in)

parameter estimation [23], and flexibility analysis [24]. While physics-informed modeling methods demonstrate advantages over traditional algorithms in efficiency, noise immunity, and accuracy, a core obstacle remains: apart from the loss function with physical laws, these deep learning methods are still black box models. The physical constraints in loss functions merely implicitly imply the presence of physical properties within the neural networks rather than providing explicit expressions of these relationships.

Considering this gap, the primary objective of this study is to introduce an interpretable spatio-temporal feature extractor for soft sensors in industrial process modeling and monitoring. We propose a spatio-temporal consistent and interpretable model (STCIM) with an encoder-decoder structure and an interpretable latent space. This method unfolds in two distinct phases: in the first stage, a root layer is designed to extract the local features at different times, and an adaptive position encoding layer is embedded into the root layer to ensure the spatio-temporal consistency. Subsequently, the spatio-temporal features are utilized as input to a far topological alignment layer, computing the correlations among the features. The potential far topological coupling will be captured to calculate the latent space. In the second stage, the latent space is guided by the first principle and integrated into the loss function to predict the output. The latent space is explicitly assigned physical properties to maintain the interpretability of the model. Notably, this methodology holds potential for adaptation to other domains within industrial modeling or diagnostic applications. The efficacy of these concepts is validated through extensive experimentation using simulated datasets and real-world data from a 330MW power plant. In summary, the key contributions of this paper encompass:

- 1) A spatio-temporal consistent and interpretable model (STCIM) is proposed for industrial process modeling and monitoring. It efficiently extracts and aligns the spatio-temporal features of industrial processes and gives the latent variables physical meanings to improve the model's interpretability.
- 2) The far topological spatio-temporal consistency extraction block is introduced to extract and align spatio-temporal features by using adaptive position encoding and attention modules.
- 3) The physics-informed interpretable latent space block is introduced to map the features into the state-space by giving explicit physical meanings to latent variables and integrating them in a discrete state-space loss function, enhancing the feature interpretability.
- 4) The efficacy of STCIM is underscored through its application experiments and ablation experiments in two simulated datasets and a real-world dataset, thus substantiating its effectiveness in practical settings.

The paper is organized as follows: Section II provides background about attention blocks, shortcut connections, and physics-informed loss functions. Section III describes the detailed information of the proposed STCIM including the far topological spatio-temporal consistency extraction block, the physics-informed interpretable latent space block, and the

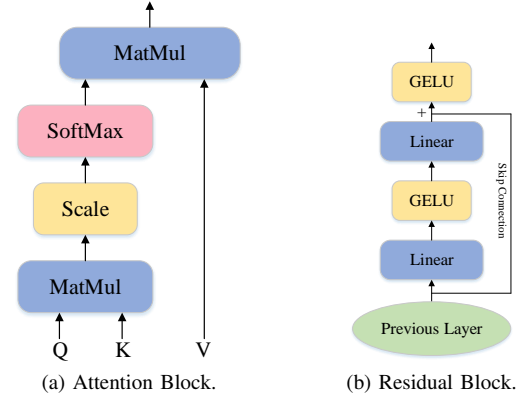


Fig. 1. The basic attention (left) and residual (right) blocks [25].

model structure. Section IV shows the experimental results, and Section V concludes the paper.

II. PRELIMINARIES

A. Attention Block

The attention block is widely used for large language models to measure the importance of each input word [25]. An attention function can be described as mapping a query and a set of key-value pairs to an output, which is shown in Figure 1a. The computation can be described as follows:

$$Attention(Q, K, V) = SoftMax\left(\frac{QK^T}{\sqrt{d_k}}\right)V \quad (1)$$

where Q , K , and V are separate sets of queries, keys, and values. $\frac{1}{\sqrt{d_k}}$ is the scaling factor. In particular, when we use the self-attention block, Q , K , and V are the same. When the input is time-series data, it can extract intrinsic temporal correlations on the timeline.

B. Shortcut connections

Difficulty introduced by the degeneracy phenomenon is always encountered in training neural networks with large depth. One of the possible solutions is the shortcut connection (residual connection), which has had great success in many applications [26]. In the aspect of information theory, the introduced shortcut connections in residual neural networks enable input data to flow directly to the next layer without information loss. It has been proven that residual neural networks can improve the performance of networks with an increase in depth. The basic residual block used in Transformer is shown in Figure 1b, and can be expressed as

$$y^l = F(y^{l-1}, W^l, b^l) + y^{l-1} \quad (2)$$

where y^l and y^{l-1} are the output of layer l and $l-1$. W^l, b^l are the weights and bias of layer l . $F(\cdot)$ is the residual function that contains the linear transformations and the Gaussian error linear unit (GELU) activation functions [27].

C. Physics-informed loss function

The physics-informed loss function is designed based on physical systems and available datasets. Assuming that the physical system can be represented as follows:

$$\begin{aligned} \text{Physical Model: } & y_{t,x} = -f(u; \theta)(x), \\ \text{Initial Conditions: } & \Psi(u; \theta)(x, t_0) = 0, \\ \text{Boundary Conditions: } & \Gamma(u; \theta)(x, t) = 0. \end{aligned} \quad (3)$$

where $y_{t,x}$ is the output of the model, f is the nonlinear function, $x \in \Omega$ is the input of model, $\Omega \in \mathbb{R}^d$, $u \in \mathbb{R}^m$ are the state variables of the system, θ is the parameters of model, and $t \in [t_0, T]$ is the time domain (all variables and parameters are vectors). For dynamic systems, initialization and boundary conditions are defined separately as $\Psi(u; \theta)$ and $\Gamma(u; \theta)$.

Considering the above physical system and assuming that we have a dataset \mathcal{D} containing all state variables $u(x)$, input variables x , time t , and output variables y , the physics-informed loss function is defined as follows:

$$Loss = L(y, \hat{y}) + \lambda R(\theta) + \gamma R_{Phy}(x, y) \quad (4)$$

where \hat{y} is the actual data, L is the Mean Square Error (MSE), $R(\theta)$ is the parametric regularization of the model (i.e. $L1$ and $L2$ norm regularization), $R_{Phy}(x, y)$ is the physical constraint loss which consists of physical models, initial conditions, and boundary conditions (i.e. $R_{Phy}(x, y) = y_{t,x} + f(u; \theta)(x)$). λ and γ are separately the hyper-parameters of the parametric regularization and physical constraint. According to Eq. (4), the physical prior knowledge in Eq. (3) is embedded in the loss function to constrain neural networks.

III. SPATIO-TEMPORAL CONSISTENT AND INTERPRETABLE MODELING

Modern multi-coupled industrial processes are composed of multiple interconnected production units that have complex material and energy transfers and intricate structures. Hence, time delay and coupling among variables in industrial processes are the main obstacles for modeling and monitoring. In this section, we introduce the proposed far topological spatio-temporal consistency extraction block and the physics-informed interpretable latent space block for the interpretable feature extraction in soft sensors.

A. Far Topological Spatio-Temporal Consistency Extraction Block

The far topological spatio-temporal consistency extraction block can be divided into two layers: the spatio-temporal feature extraction layer and the far topological alignment layer.

1) *Spatio-Temporal Feature Extraction Layer*: Figure 2 describes the spatio-temporal feature extraction layer. The input data, respectively, pass through a temporal feature extraction layer and an adaptive position encoding layer to capture the local features from different times and locations. The massive local spatio-temporal features ensure the abundance of far topological variables.

Assume that the input variables at time t are $X(t) \in \mathbb{R}^{H \times W \times C}$ where H , W , and C are separately the backtracking

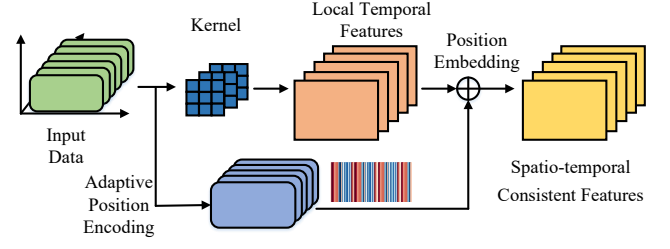


Fig. 2. Spatio-temporal consistent block.

from time t , the number of features, and the number of input channels ($C = 1$). $X(t)$ can be expressed as

$$X(t) = \begin{bmatrix} x_1(t - (H-1) \times T) & x_2(t - (H-1) \times T) & \cdots & x_n(t - (H-1) \times T) \\ \vdots & \vdots & \ddots & \vdots \\ x_1(t - 2 \times T) & x_2(t - 2 \times T) & \cdots & x_n(t - 2 \times T) \\ x_1(t - 1 \times T) & x_2(t - 1 \times T) & \cdots & x_n(t - 1 \times T) \\ x_1(t) & x_2(t) & \cdots & x_n(t) \end{bmatrix} \quad (5)$$

where T is the sampling time. When different convolution kernels are applied in $X(t)$, the local features of adjacent attributes and times are extracted, reflecting the dynamics of the industrial process. However, these features come from different attributes at different times, lacking the corresponding spatial features. To overcome the problem, inspired by [28], an adaptive position encoding method is given by

$$Position_i = \frac{Variable_i}{\sqrt{N}} \quad (6)$$

where $Variable_i$ is the trainable position parameter of i_{th} attributes. N is the number of features that is a scaling factor. $Position_i$ is the position encoding of the i_{th} attributes. Due to the unknown time delay and coupling among variables in industrial processes, fixed position encoding is not appropriate, for example, 'sin' and 'cos' encoding. The trainable position parameter $Variable_i$ in this layer can adaptively ensure spatio-temporal consistency of captured local features.

2) *Far Topological Alignment Layer*: During the industrial process, variables are related not only to adjacent nodes but also to variables in far topological structures. Aligning the topological correlation among spatio-temporal local features is vital for industrial process modeling and monitoring. In this vein, we propose a far topological alignment layer, which is shown in Figure 3. This layer is coupled with the spatio-temporal feature extraction layer. Local spatio-temporal features are sparsely mapped and aligned by multi-head attention modules to capture the topological correlation in industrial processes. The calculated attention weights can be considered as the dependencies among far topological features and captured by models. Subject to potential far topological variable correlations, the adaptive position encoding at the spatio-temporal feature extraction layer is realigned with new features, which will again improve the modeling and monitoring accuracy.

Assume that the features captured by the spatio-temporal feature extraction layer are $V \in \mathbb{R}^{H \times W \times K}$. Based on the

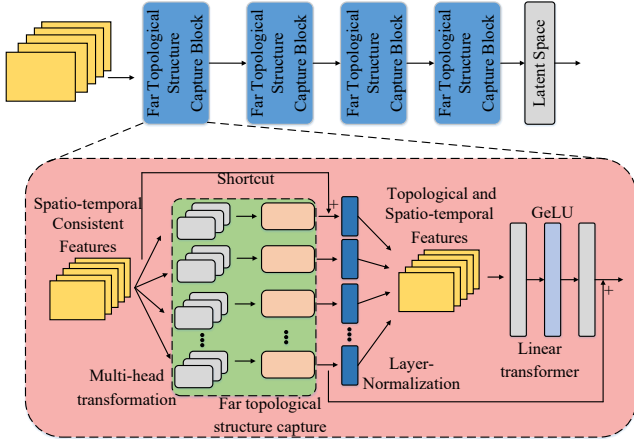


Fig. 3. Far topological structure capture block.

attention weights in Eq. (1), the dependencies among far topological features can be calculated by

$$Weight(V, V) = SoftMax\left(\frac{VV^T}{\sqrt{d_k}}\right) \quad (7)$$

where $Q = K = V$. The calculated weights determine the intrinsic correlation among the input features, helping the networks capture the potential far topological structure among all the features. By multiplying $Weight(V, V)$ with V , the importance determined by the long-term topological correlation can be used in feature extraction.

B. physics-informed Interpretable Latent Space Block

To limit the captured features in first principles and map these sparse features into an interpretable state-space, this subsection introduces the physics-informed interpretable latent space block by giving physical meanings to the latent space z of STCIM. We can directly relate the inputs, latent variables, and outputs by the physics-informed discrete state-space loss function and boundary conditions. Here, we need to highlight that the latent space z is an intermediate process parameter instead of the input of STCIM. It can be unobserved or hard to measure.

Assuming the discrete-time state-space equation and output equation of the industrial process are given by

$$u(k) = \Phi(u(k-1), \theta_1) + G(x(k), \theta_2) \quad (8)$$

$$y(k) = H(u(k), \theta_3) + J(x(k), \theta_4) \quad (9)$$

where x is the input, u is the unobserved state variables, and y is the output. $\Phi(\cdot)$, $G(\cdot)$, $H(\cdot)$, $J(\cdot)$ are separately the non-linear operators. θ is the parameter. All variables are vectors. Now, we can map the discrete-time state-space equation into STCIM. Assuming that the latent space z of STCIM is the state variables at time $k-1$ and k ($z_1 = u(k)$, $z_2 = u(k-1)$) and $z = [z_1, z_2]$ and the input and output of the STCIM are x and \hat{y} , respectively. Then, the discrete state-space loss function of STCIM can be given by

$$Loss = L(y, \hat{y}) + \lambda R(\theta) + \gamma_1(\hat{y} - H(z_1, \theta_3) - J(u, \theta_4)) + \gamma_2(z_1 - \Phi(z_2, \theta_1) - G(x, \theta_2)) \quad (10)$$

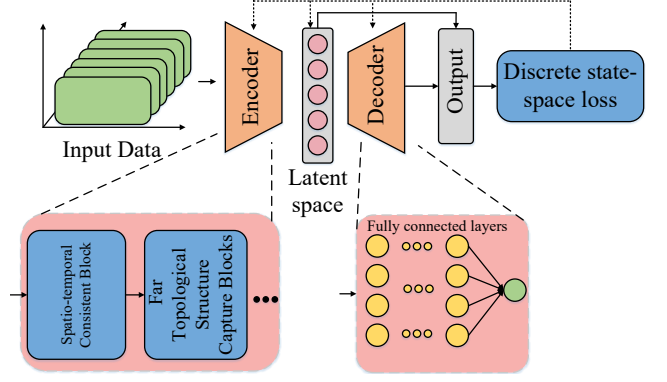


Fig. 4. Spatio-temporal consistent and interpretable model.

where γ is the weight coefficient. When the $\gamma = [\gamma_1, \gamma_2] \rightarrow \infty$, the STCIM completely trusts the state-space model. In contrast, when the $\gamma = [\gamma_1, \gamma_2] \rightarrow 0$, the STCIM is a data-driven model without physical prior knowledge. By balancing the tendencies towards data-driven and physics-driven models, STCIM can achieve the trade-off in the loss function. According to Eq. (10), the discrete state-space loss function consists of four sub-losses: 1) the MSE loss $L(y, \hat{y})$, 2) the parametric regularization of the model $R(\theta)$, 3) the output equations loss $\hat{y} - H(z_1, \theta_3) - J(x, \theta_4)$, 4) the state equation loss $z_1 - \Phi(z_2, \theta_1) - G(x, \theta_2)$. Although the state variables are not measurable, the neural network will output the actual state variables because the latent space is constrained at both sub-losses 3 and 4, which provides physical properties.

C. Model Structure

Figure 4 shows the structure of the spatio-temporal consistent and interpretable model. It can be recognized as an encoder-decoder structure, which is generally considered as a feature extractor and a function fitter when applied in many aspects. The idea of the model can be summarized as compressing the spatio-temporal consistent features with high dimensions into an interpretable latent space, which normally has fewer dimensions, and then the interpretable latent variables are utilized to fit the potential mathematical equations.

As aforementioned, the far topological spatio-temporal consistency extraction block is used as the encoder to capture and align the far topological spatio-temporal features among variables. The decoder is composed of MLPs, which is enough for discrete function fitting. The latent variables and the outputs are endowed with physical meanings by using a physics-informed interpretable latent space block. The size of the latent space is determined by the form of discrete state-space equations, e.g., if there are two state variables in a discrete model, then the number of latent variables for STCIM is four because it contains the state variables at time k and $k-1$.

IV. EXPERIMENTAL RESULTS

To validate the efficiency of our method, we test the proposed STCIM in three stages. First, analytical experiments based on two generated datasets are used to demonstrate

TABLE I
THE PRM OF MAIN MODELS. #PRM DENOTES THE NUMBER OF
PARAMETERS.

Models	STCIM	PhyLSTMs [24]	PIML [29]	VCACNN [7]	MSACNN [10]
#PRM	0.023M	0.428M	0.025M	0.371M	0.082M

the effectiveness of STCIM. Then, a real-life dataset from a 330MW power plant is utilized as a comparative experiment to further validate the robustness and efficiency of STCIM. At last, we emphasize the importance of position encoding, far topological coupling among variables, and hyper-parameters in the loss function.

A. Experiment Setup

The utilized datasets contain two generated datasets and one real-world dataset. The two generated datasets include a reduced rotary speed dataset and a 3-order synchronous generator dataset, which are both important for the equipment of industrial processes. The comparative experiment has a 330MW coal-fired power plant dataset that reflects a complex industrial process with heat and mass transformation. All the datasets have two operation conditions, and each condition has at least 50,000 points with noise. The model is trained in one operation condition and tested in another to highlight the effectiveness of STCIM. The state variables are not used as input to models.

For each STCIM block, we have different parameters. In the spatio-temporal feature extraction layer block, the features are extracted by two 2D-convolution layers with 64 filters, and each kernel is 3×3 . The far topological alignment layer has four heads, and each head has three linear transformations, and each linear layer has 256 neurons. The number of interpretable variables is chosen based on the real physical model. For the decoder, each fully connected layer has 256 neurons and GeLU as an activation function. For all experiments, γ_1 and γ_2 in Eq. (10) are set as 1 and 0.5 separately. During the training process, the latent variables and the target output of STCIM will be integrated into the discrete state-space loss function and then collaboratively optimized by the backpropagation algorithm.

Four more deep learning-based soft sensor modeling methods are explored for comparisons, including two different PINN-based models [24], [29], and two CNN-based models [7], [10], since they have demonstrated their out-performance in soft sensor. Table I shows the number of parameters of models. For each experiment, we train the models with a batch size of 64 or 128 using the ‘NAdam’ optimizer with an initialized learning rate of 0.01. The learning rate decays by a factor of 0.1 every 30 epochs. The max epoch is set to 100. The experiments are implemented in Tensorflow using a CPU Intel i7-11800H CPU at 2.3Hz and an NVIDIA T600 GPU.

B. Analytical Experiments

In this section, we use two equipment models with different levels of difficulty to demonstrate the reliability and scalability

of STCIM in modeling and condition monitoring. For long-time-series datasets, STCIM can be used not only in complex industrial processes, but also in relatively simple equipment monitoring without over-fitting. The well-designed modules improve the accuracy of the modeling and monitoring.

1) *Rotor Equation-Reduced Rotary Speed*: The stability of the rotor is one of the key factors for the stable operation of the micro gas turbine. During the operation of the micro gas turbine, the rotor needs to maintain a certain speed and stability to ensure the normal operation of the machine. If the rotor vibrates or becomes unstable, it will have a negative impact on the operation of the micro gas turbine and may even cause damage to the machine. Therefore, the modeling and monitoring of the rotor need to be fully considered.

The corresponding reduced rotary speed can be calculated by the rotor equation and its transformation, which is given by

$$\frac{dn}{dt} = \frac{900}{\pi^2 J n} (N_T - N_C),$$

$$\hat{n} = \frac{n}{\sqrt[2]{\frac{T_1}{288}}}. \quad (11)$$

where n is the rotor speed, J is the rotary inertia, \hat{n} is the output reduced rotary speed, T_1 is the air temperature and N_T and N_C are separately the generated power by the turbines and consumed power by the compressor. The generated dataset contains all the inputs, outputs, and states with 80,000 points with noise.

Table II shows that in the analytical experiment, the STCIM completely outperforms all the other physics-based deep learning models and CNN-based models. The evaluation metrics of STCIM are much smaller than the evaluation metrics of other models, indicating the superiority of STCIM.

TABLE II
EVALUATION METRICS OF THE REDUCED ROTARY SPEED

Evaluation		STCIM	PhyLSTMs [24]	PIML [29]	VCACNN [7]	MSACNN [10]
MAE	\hat{n}	0.14	0.79	1.24	0.24	0.85
	n	0.16	1.03	1.33	0.26	0.75
MSE	\hat{n}	0.03	1.01	2.28	0.10	0.46
	n	0.04	1.68	2.57	0.12	0.63
MAPE (10^{-3}) (%)	\hat{n}	5.18	28.82	45.25	8.93	15.35
	n	5.73	36.84	41.59	9.32	28.64

2) *3 Order Synchronous Generator*: The synchronous generator is the core equipment in the power system, responsible for converting mechanical energy into electrical energy. Its stable operation is directly related to the power supply quality and reliability of the entire power system. At the same time, since the synchronous generator can stably output the required voltage by adjusting the excitation current, and the rotor is synchronized with the power grid, it is crucial to protect power equipment and ensure the stability of the power supply.

A 3-order synchronous generator is a practical model that has been widely used in modeling and monitoring. We leverage the classic 3-order synchronous generator as the simulation

model, which is given as follows for data generation.

$$\begin{aligned}
T'_{do} \frac{d\hat{E}_q}{dt} &= E_f - \hat{E}_q - (x_d - x'_d)i_d, \\
T_J \frac{dw}{dt} &= P_m - [\hat{E}_q i_q - (x'_d - x_q)i_d i_q], \\
\frac{d\delta}{dt} &= w - 1, \\
u_d &= x_q i_q - r_a i_d, \\
u_q &= \hat{E}_q - x'_d i_d - r_a i_q.
\end{aligned} \tag{12}$$

where i is the input current, u is the output voltage, w is the angular velocity and \hat{E}_q is the transient internal voltage. Since δ is not related to outputs, it will be ignored in our case. Other parameters are constants. The generated dataset contains all the generated currents, voltages, angular velocity, and power with 50,000 points for each operation condition.

The Table III shows the evaluation of the state estimation (w, \hat{E}_q) and output regression (i_q, i_d) across five different architectures. The proposed STCIM outperforms the other deep learning methods among most evaluation metrics, especially in the output regression and w estimation. Compared with other models, the performance of \hat{E}_q estimation of STCIM is comparable.

TABLE III
EVALUATION METRICS OF THE 3-ORDER SYNCHRONOUS GENERATOR

Evaluation		STCIM	PhyLSTMs [24]	PIML [29]	VCACNN [7]	MSACNN [10]
MAE (10^{-2})	i_q	3.38	3.45	3.57	3.41	3.66
	i_d	3.63	4.07	4.23	3.78	4.05
	w	9.18	16.94	12.51	10.27	11.03
	\hat{E}_q	1.46	1.45	1.47	1.42	1.33
MSE (10^{-3})	i_q	1.75	1.79	1.88	1.80	1.99
	i_d	2.08	2.55	2.73	2.62	2.72
	w	13.12	46.30	57.13	36.78	18.05
	\hat{E}_q	0.32	0.35	0.34	0.35	0.36
MAPE (%)	i_q	4.15	4.24	4.38	4.26	4.47
	i_d	27.03	28.44	29.32	28.01	27.21
	w	9.18	16.93	17.29	16.87	11.02
	\hat{E}_q	1.52	1.52	1.48	1.51	1.49

C. Comparative Experiments

This section is used to demonstrate the effectiveness of STCIM in long-time-series datasets of complex industrial processes. The real-life dataset comes from a 330MW coal-fired power plant, which is shown in Figure 5. The processes of coal-fired power plants are multifaceted and complex, including chemical reactions, energy conversion, mass transfer, and phase changes. The utilized 330MW power plant [30] can be given by

$$\begin{aligned}
r'_B &= e^{-18s} u_B \\
120 \frac{dr_B}{dt} &= -r_B + r'_B \\
3266 \frac{dp_d}{dt} &= -0.2501 p_t u_T + 6.77 r_B \\
12 \frac{dN_E}{dt} &= -N_E + 0.2501 p_t u_T \\
p_t &= p_d - 0.0004555 (6.77 r_B)^{1.3}
\end{aligned} \tag{13}$$

where u_B is the fuel signal (kg/s), u_T is the opening of turbine (%), r_B is the actual fuel (kg/s), p_d is the pressure of

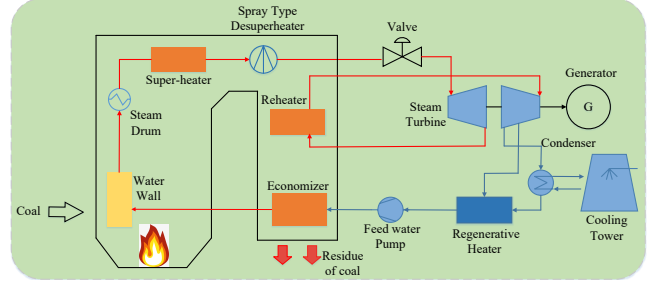


Fig. 5. 330MW coal power plant.

steam (MPa) and N_E is the output power (MW). $z_1 = \frac{dr_B}{dt}$, $z_2 = \frac{dp_d}{dt}$ and $\dot{y} = \frac{dN_E}{dt}$.

To verify the generalization of STCIM, it is tested under both the same operation condition (Test 1) and a different operation condition (Test 2). Figure 6 shows the outputs and state estimation of the real-life dataset. To reveal the performance of STCIM, 400 points in the test dataset are selected in the figures. Table IV compares the STCIM with four other deep learning models in the dataset. Compared with Figure 6a, the performance of STCIM in Figure 6b is better owing to the obvious fluctuations in state variables and the detailed information from sub-devices. As depicted in the Figures, the changes in output power and the amount of coal are larger, promoting the learning of system dynamic characteristics by STCIM. The test of STCIM under the same operation conditions shown in Figure 6a has good performance, including the forecasting of state variables. Meanwhile, STCIM maintains good generalization ability in prediction under a new operation condition.

Table IV shows the evaluation metrics among the five deep learning models in both Test 1 and Test 2. When the models are tested under the same operation condition, the performance of all the tested models is similar. Some models can outperform STCIM in some specific evaluation metrics because the dataset under the same operation condition has similarity, for example, noise in the output. To pursue better generalization, STCIM pays more attention to consistent spatio-temporal features and meaningful latent variables rather than the noise. In contrast, under another operation condition, the generality of STCIM is much better than that of other models. All evaluation metrics for all power prediction and latent variables prediction by STCIM are smaller than other methods, implying the effectiveness of STCIM.

D. Ablation Experiments

In this section, we discuss the importance of spatio-temporal consistency and the hyper-parameters of the physics-informed interpretable latent space block in STCIM. The real-life dataset is utilized in ablation experiments. The setup is the same as in comparative experiments.

1) *The importance of spatio-temporal consistency:* In this experiment, we emphasize the importance of spatio-temporal consistency by comparing models with and without position encoding using a real-life dataset, which is shown in Figure 7. Compared with Figure 6, there is little difference in output y

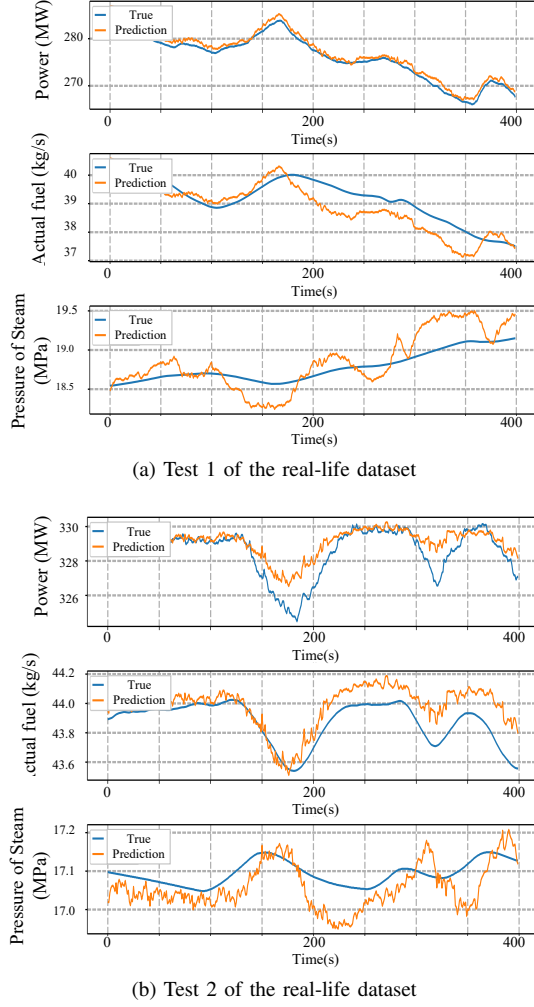
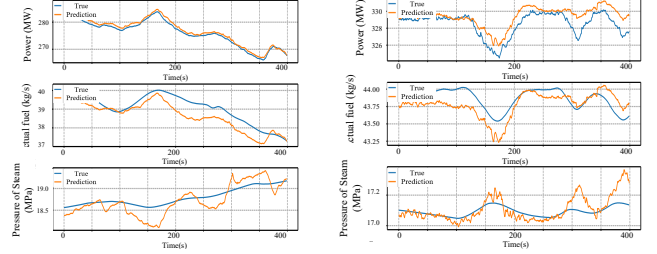


Fig. 6. The outputs and latent variables of comparative experiments

TABLE IV
EVALUATION METRICS OF THE REAL-LIFE DATASET

Evaluation		STCIM	PhyLSTMs [24]	PIML [29]	VCACNN [7]	MSACNN [10]
MAE (Test 1)	y	0.45	0.41	0.40	0.46	0.78
	z_1	0.43	0.76	0.61	0.44	1.07
	z_2	0.18	0.21	0.69	0.18	0.51
MSE (Test 1)	y	0.31	0.29	0.26	0.31	1.01
	z_1	0.25	0.87	0.59	0.29	1.73
	z_2	0.05	0.08	1.71	0.06	0.43
MAPE (Test 1, %)	y	0.37	0.26	0.25	0.45	0.78
	z_1	1.20	1.98	1.58	1.12	2.77
	z_2	0.98	1.12	1.61	0.99	2.66
MAE (Test 2)	y	0.46	0.54	0.57	0.46	0.75
	z_1	0.11	0.56	0.14	0.28	0.68
	z_2	0.05	0.05	1.38	0.11	0.26
MSE (Test 2)	y	0.49	0.50	0.67	1.08	0.94
	z_1	0.02	0.07	0.03	0.05	0.07
	z_2	0.03	0.04	0.07	0.16	0.09
MAPE (Test 2, %)	y	0.14	0.15	0.21	0.48	0.23
	z_1	0.35	0.65	0.35	0.44	0.55
	z_2	0.33	0.34	0.54	0.67	0.61

forecasting under the same operation condition. However, the predicted state variables without adaptive position encoding are not as accurate as the model with it. A similar situation appears in Test 2. The volatility of all the predicted variables, including latent variables and output, is greater than that of the model with position encoding, especially in actual fuel



(a) Test 1 for the real-life dataset without position encoding (b) Test 2 for the real-life dataset without position encoding

Fig. 7. The outputs and latent variables of experiments in a real-life dataset without position encoding.

TABLE V
EVALUATION METRICS OF EXPERIMENTS IN REAL-LIFE DATASET WITHOUT POSITION ENCODING

Datasets	MSE			MAE			MAPE (%)		
Type	y	z_1	z_2	y	z_1	z_2	y	z_1	z_2
Test 1	0.83	0.35	0.06	0.81	0.47	0.15	0.38	1.20	1.12
Test 2	1.37	0.06	0.06	0.98	0.21	0.09	2.90	1.48	0.54

forecasting. The bias between field data and predicted actual fuel in Figure 7b is much greater than that in Figure 6b.

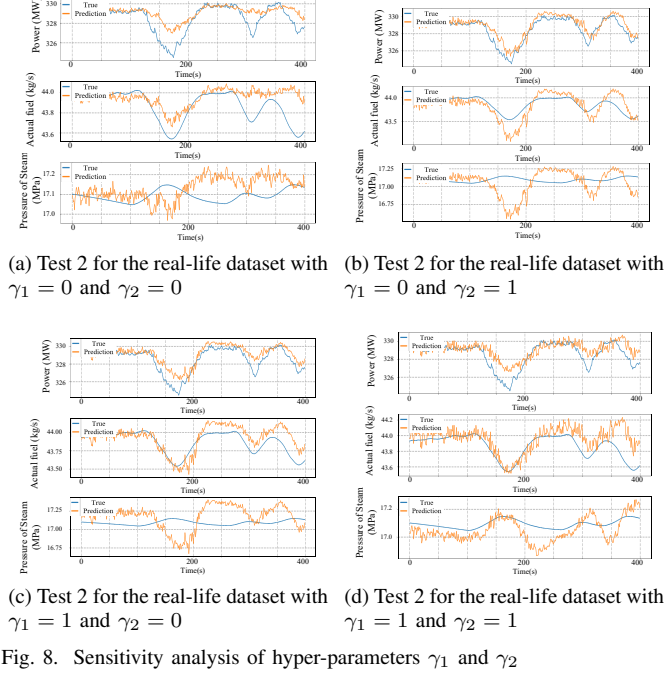
Table V shows the evaluation metrics of experiments in the real-life dataset without adaptive position encoding. Compared with Table IV, Test 1 with or without position encoding has similar performance. Nevertheless, the generalization of the model without adaptive position encoding in Test 2 is worse compared to the model performance in Table IV. For example, the MSE in y forecasting without adaptive position encoding almost triples compared with the model with adaptive position encoding. The improvement of generalization benefits from adaptive position encoding. By position encoding, the features are endowed with additional information, which improves the expressiveness of STCIM.

2) *The importance of far topological alignment*: By replacing the far topological alignment layer with a CNN model, we emphasize the necessity of the far topological alignment layer in STCIM. Since power generation in a power plant is a very complex industrial process, the input variables are coupled with each other. At the same time, the inertia of each device causes the spatial and temporal data to be misaligned, affecting the accuracy of modeling. Table VI describes how the evaluation metrics change when the far topological alignment is replaced. All evaluation metrics become worse at both test 1 and test 2, especially in the y prediction. The lack of far topological alignment makes the model focus more on local features, while ignoring the potential dependencies of far topological correlations of variables, reducing the accuracy of modeling and monitoring, which is fatal for a large and complex industrial process.

3) *Sensitivity Analysis of hyper-parameters γ* : The impact of hyper-parameters γ_1 and γ_2 on performance of STCIM are tested in this part. Figure 8 shows the performance of STCIM using different γ . When the state equations are not considered in the loss function, the output y and state variables

TABLE VI
EVALUATION METRICS OF EXPERIMENTS IN A REAL-LIFE DATASET
WITHOUT FAR TOPOLOGICAL ALIGNMENT

Datasets	MSE			MAE			MAPE (%)		
Type	y	z_1	z_2	y	z_1	z_2	y	z_1	z_2
Test 1	0.97	0.42	0.06	0.90	0.51	0.32	0.46	1.38	1.45
Test 2	1.78	0.13	0.09	1.08	0.32	0.09	2.93	1.56	0.82



are unable to align with actual data. Additionally, the utilized part of the state equations can partly guarantee the fit of state variables. The complexity of the expression determines which state variable is automatically fitted by the neural network. When $\gamma_1 = 1$ and $\gamma_2 = 1$, there is more oscillation in Figure 8d compared with Figure 6b since more loss about state variables are considered in physics-informed interpretable latent space block.

V. CONCLUSION

As modern industrial processes become complex, general soft sensor methods are gradually unable to meet the requirements. This paper introduces a novel soft sensor method termed spatio-temporal consistent and interpretable model (STCIM). We designed a far topological spatio-temporal consistency extraction block to capture and align temporal and spatial features from raw data. Subsequently, by giving physical meanings to latent variables and integrating them in a physics-informed discrete state-space loss function, the physics-informed interpretable latent space block maps the spatio-temporal features to an interpretable state-space to improve the feature interpretability. The primary outcome underscores the STCIM's capability to effectively extract and align the spatio-temporal features and the far topological structure. The analytical experiments underscore that STCIM has robust generalization performance across diverse operational

conditions, particularly when the training dataset exhibits significant fluctuations in both outputs and state variables, thereby enabling informed and reliable decision-making among power domain experts. The ablation experiments highlight the critical significance of adaptive position encoding, the far topological alignment, and the hyper-parameters of the loss function.

The key limitation of the approach lies in its dependence on prior knowledge of the loss function. When more intricate state-space equations are incorporated into the model, part of the equations can lead to gradient disappearance. Nonetheless, we believe that STCIM has considerable potential for explicitly elucidating the neural network operations. Therefore, there may be significant room for future research, which may focus on the combination of physical models and neural networks.

REFERENCES

- [1] Y. Jiang, S. Yin, J. Dong, and O. Kaynak, "A review on soft sensors for monitoring, control, and optimization of industrial processes," *IEEE Sensors Journal*, vol. 21, no. 11, pp. 12 868–12 881, 2021.
- [2] B. Huang, Y. Qi, and A. M. Murshed, "Dynamic modelling and predictive control in solid oxide fuel cells: First principle and data-based approaches: Huang/dynamic modelling and predictive control in solid oxide fuel cells: First principle and data-based approaches," 2013.
- [3] X. Yuan, N. Xu, L. Ye, K. Wang, F. Shen, Y. Wang, C. Yang, and W. Gui, "Attention-based interval aided networks for data modeling of heterogeneous sampling sequences with missing values in process industry," *IEEE Transactions on Industrial Informatics*, vol. 20, no. 4, pp. 5253–5262, 2024.
- [4] R. Guo, H. Liu, G. Xie, Y. Zhang, and D. Liu, "A self-interpretable soft sensor based on deep learning and multiple attention mechanism: From data selection to sensor modeling," *IEEE Transactions on Industrial Informatics*, vol. 19, no. 5, pp. 6859–6871, 2023.
- [5] Q. Sun and Z. Ge, "A survey on deep learning for data-driven soft sensors," *IEEE Transactions on Industrial Informatics*, vol. 17, no. 9, pp. 5853–5866, 2021.
- [6] H. Wu, X. Chen, P. Li, and Z. Wen, "Automatic symmetry detection from brain mri based on a 2-channel convolutional neural network," *IEEE Transactions on Cybernetics*, vol. 51, no. 9, pp. 4464–4475, 2021.
- [7] X. Yuan, Y. Wang, C. Wang, L. Ye, K. Wang, Y. Wang, C. Yang, W. Gui, and F. Shen, "Variable correlation analysis-based convolutional neural network for far topological feature extraction and industrial predictive modeling," *IEEE Transactions on Instrumentation and Measurement*, vol. 73, pp. 1–10, 2024.
- [8] S. Zou, K. Li, Z. Li, F. Huang, and L. Chen, "A soft sensor model based on rime-tcn-bigru-attention for predicting heavy calcium carbonate particle size distribution," *IEEE Transactions on Instrumentation and Measurement*, vol. 74, pp. 1–13, 2025.
- [9] X. Yuan, S. Qi, Y. Wang, and H. Xia, "A dynamic cnn for nonlinear dynamic feature learning in soft sensor modeling of industrial process data," *Control Engineering Practice*, vol. 104, p. 104614, 2020.
- [10] X. Yuan, L. Huang, L. Ye, Y. Wang, K. Wang, C. Yang, W. Gui, and F. Shen, "Quality prediction modeling for industrial processes using multiscale attention-based convolutional neural network," *IEEE Transactions on Cybernetics*, vol. 54, no. 5, pp. 2696–2707, 2024.
- [11] X. Yuan, L. Li, Y. A. W. Shardt, Y. Wang, and C. Yang, "Deep learning with spatiotemporal attention-based lstm for industrial soft sensor model development," *IEEE Transactions on Industrial Electronics*, vol. 68, no. 5, pp. 4404–4414, 2021.
- [12] T. Zhang, X. Gong, and C. L. P. Chen, "Bmt-net: Broad multitask transformer network for sentiment analysis," *IEEE Transactions on Cybernetics*, vol. 52, no. 7, pp. 6232–6243, 2022.
- [13] J. Xue, K. Li, T. Zhang, and H. Ye, "Data-driven soft sensor for hot strip mill process based on multiscale information-fusion attention network," *IEEE Transactions on Instrumentation and Measurement*, vol. 73, pp. 1–11, 2024.
- [14] B. Pu, J. Liu, Y. Kang, J. Chen, and P. S. Yu, "Mvstt: A multiview spatial-temporal transformer network for traffic-flow forecasting," *IEEE Transactions on Cybernetics*, vol. 54, no. 3, pp. 1582–1595, 2024.
- [15] X. Yuan, S. Qi, and Y. Wang, "Stacked enhanced auto-encoder for data-driven soft sensing of quality variable," *IEEE Transactions on Instrumentation and Measurement*, vol. 69, no. 10, pp. 7953–7961, 2020.

- [16] Y. Wang, Q. Sui, C. Liu, K. Wang, X. Yuan, and G. Dong, "Interpretable prediction modeling for froth flotation via stacked graph convolutional network," *IEEE Transactions on Artificial Intelligence*, vol. 5, no. 1, pp. 334–345, 2024.
- [17] L. Kong, C. Yang, S. Lou, Y. Cai, X. Huang, and M. Sun, "Collaborative extraction of intervariable coupling relationships and dynamics for prediction of silicon content in blast furnaces," *IEEE Transactions on Instrumentation and Measurement*, vol. 72, pp. 1–13, 2023.
- [18] L. Ma, M. Wang, and K. Peng, "A spatiotemporal industrial soft sensor modeling scheme for quality prediction with missing data," *IEEE Transactions on Instrumentation and Measurement*, vol. 73, pp. 1–10, 2024.
- [19] M. Raissi, P. Perdikaris, and G. Karniadakis, "Physics-informed neural networks: A deep learning framework for solving forward and inverse problems involving nonlinear partial differential equations," *Journal of Computational Physics*, vol. 378, pp. 686–707, 2019. [Online]. Available: <https://www.sciencedirect.com/science/article/pii/S0021999118307125>
- [20] H. Meskhidze, "Beyond classification and prediction: The promise of physics-informed machine learning in astronomy and cosmology," February 2024, forthcoming in: Juan Durán and Giorgia Pozzi (Eds.) *Philosophy of Science for Machine Learning: Core Issues and New Perspective*, Synthese Library. [Online]. Available: <https://philsci-archive.pitt.edu/23067/>
- [21] B. Huang and J. Wang, "Applications of physics-informed neural networks in power systems - a review," *IEEE Transactions on Power Systems*, vol. 38, no. 1, pp. 572–588, 2023.
- [22] A. Daw, A. Karpatne, W. Watkins, J. Read, and V. Kumar, "Physics-guided neural networks (pgnn): An application in lake temperature modeling," 2021.
- [23] W. Wang and N. Yu, "Estimate three-phase distribution line parameters with physics-informed graphical learning method," *IEEE Transactions on Power Systems*, vol. 37, no. 5, pp. 3577–3591, 2022.
- [24] M. Lahariya, F. Karami, C. Develder, and G. Crevecoeur, "Physics-informed lstm network for flexibility identification in evaporative cooling system," *IEEE Transactions on Industrial Informatics*, vol. 19, no. 2, pp. 1484–1494, 2023.
- [25] A. Vaswani, N. Shazeer, N. Parmar, J. Uszkoreit, L. Jones, A. N. Gomez, L. Kaiser, and I. Polosukhin, "Attention is all you need," 2023.
- [26] K. He, X. Zhang, S. Ren, and J. Sun, "Deep residual learning for image recognition," 2015.
- [27] D. Hendrycks and K. Gimpel, "Gaussian error linear units (gelus)," 2023.
- [28] A. Dosovitskiy, L. Beyer, A. Kolesnikov, D. Weissenborn, X. Zhai, T. Unterthiner, M. Dehghani, M. Minderer, G. Heigold, S. Gelly, J. Uszkoreit, and N. Houlsby, "An image is worth 16x16 words: Transformers for image recognition at scale," 2021.
- [29] J. Kruse, E. Cramer, B. Schäfer, and D. Witthaut, "Physics-informed machine learning for power grid frequency modeling," *PRX Energy*, vol. 2, p. 043003, Oct 2023. [Online]. Available: <https://link.aps.org/doi/10.1103/PRXEnergy.2.043003>
- [30] Q. Wang, L. Pan, Z. Liu, H. Wang, X. Wang, and W. Tang, "Interpretable uncertainty forecasting framework for robust configuration of energy storage in a virtual power plant," *Journal of Energy Storage*, vol. 84, p. 110800, 2024. [Online]. Available: <https://www.sciencedirect.com/science/article/pii/S2352152X24003840>